

## Synthesis of magnetic photocatalyst by photochemical deposition and co-precipitation techniques: investigation of its photocatalytic and sonophotocatalytic activity for dye removal

Asmaa Ghazi Jameel Alwindawi, Mehmet Turkyilmaz & Sezen Kucukcongar

**To cite this article:** Asmaa Ghazi Jameel Alwindawi, Mehmet Turkyilmaz & Sezen Kucukcongar (2022) Synthesis of magnetic photocatalyst by photochemical deposition and co-precipitation techniques: investigation of its photocatalytic and sonophotocatalytic activity for dye removal, International Journal of Environmental Analytical Chemistry, 102:19, 8419-8433, DOI: 10.1080/03067319.2020.1849657

**To link to this article:** <https://doi.org/10.1080/03067319.2020.1849657>



Published online: 23 Nov 2020.



Submit your article to this journal [↗](#)



Article views: 285



View related articles [↗](#)



View Crossmark data [↗](#)



Citing articles: 2 View citing articles [↗](#)



# Synthesis of magnetic photocatalyst by photochemical deposition and co-precipitation techniques: investigation of its photocatalytic and sonophotocatalytic activity for dye removal

Asmaa Ghazi Jameel Alwindawi<sup>a</sup>, Mehmet Turkyilmaz<sup>b</sup> and Sezen Kucukcongar<sup>b</sup>

<sup>a</sup>Department of Environment and Pollution, Northern Technical University, Kirkuk, Iraq; <sup>b</sup>Department of Environmental Engineering, Konya Technical University, Konya, Turkey

## ABSTRACT

In this study, photochemical deposition and co-precipitation methods were used to synthesise Ag/TiO<sub>2</sub> and magnetic Ag/TiO<sub>2</sub>/Fe<sub>3</sub>O<sub>4</sub> photocatalysts, respectively. The physical and chemical properties of the Ag/TiO<sub>2</sub> and Ag/TiO<sub>2</sub>/Fe<sub>3</sub>O<sub>4</sub> photocatalysts were characterised by X-ray Diffraction (XRD), Scanning Electron Microscopy (SEM) and Fourier Transform Infrared Spectroscopy (FT-IR) analyses. The synthesised photocatalysts were used to remove Reactive Red 195 (RR195) dye the most commonly used in the textile industry. The photocatalytic and sonophotocatalytic removal was investigated using different light types such as UV-A and visible light. In the optimum conditions (UV-A and visible light intensity 27 W, 25 mg/L initial RR195 concentration, pH 6 ve 0.1 g/L catalyst dose) of photocatalysis, the photodegradation of magnetic Ag/TiO<sub>2</sub>/Fe<sub>3</sub>O<sub>4</sub> was found 72% at 120 min irradiation of visible light but the degradation was 65% at 30 min irradiation of UV-A light. While in case of the sonophotocatalysis, the degradation of magnetic Ag/TiO<sub>2</sub>/Fe<sub>3</sub>O<sub>4</sub> was found 85% at 120 min irradiation of visible light but the degradation was 85% at 30 min irradiation of UV-A light.

## ARTICLE HISTORY

Received 14 September 2020  
Accepted 3 November 2020

## KEYWORDS

Photocatalysis;  
sonophotocatalysis; ag/TiO<sub>2</sub>;  
ag/TiO<sub>2</sub>/Fe<sub>3</sub>O<sub>4</sub>; reactive dye  
removal; magnetic  
photocatalyst

## 1. Introduction

Dyes are a group of complex organic substances, which soak up light at the visible light region with the wavelength of 350–700 nm and classified into 20–30 groups depending on their chemical structures or chromophores [1]. Dye source can be comprised by the drainages of chemicals operation industry, for example, textiles, plastic, ceramic, ink, etc [2]. At the same time, the disposal which produced from these industries considered as a significant source of environmental pollution particularly pollution of water [3].

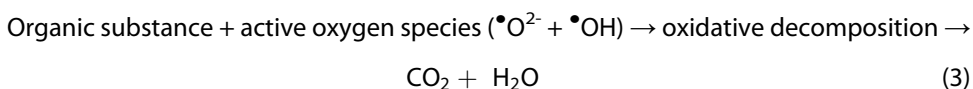
Textile is one of the most substantial industry for many countries, for example, China, Singapore, UK, Italy, Turkey etc [4]. In Turkey, the textile is a standout amongst the most energetic, greatest industry and consume a quantity of water, because of many strategies and technologies applied in this sector [5]. During the various stages of the textile industry, dye plant is the most toxic phase. The textile industry alone records for two-thirds of the whole

dye stuff generation [6]. The textile industries widely use synthetic colours in the colouring and printing process. The synthetic colours represent the main part of our lives because it's broadly used by different industries. Many of the synthetic dyes, particularly azo dye, were found to be harmful, carcinogenic and mutagenic and are accordingly restricted all through the world [7].

The researchers have discussed dyes more, due to their high dissolvability in water and as effluents containing environmentally dangerous materials. Dyes may have severe and inveterate impacts on the exposed living thing depending on an exposure time in addition to concentration of dye as well as cause allergic dermatitis, skin agitation, mutation, and several another illness [8]. Also, the existence of a slight quantity of colours (under 1 ppm) is obviously visible as well as impact the aqueous environment significantly [2].

Numerous treatment processes have been considered for the removal of dye, running from conventional techniques to the most developed advanced oxidation processes [9–15]. Hence, more consideration is given to improving treatment efficiency techniques for the degeneration of dye from the effluent of textile industry. Chemical techniques, particularly advanced oxidation processes (AOPs) like photocatalytic oxidation, sonolysis, Fenton and photo-Fenton reactions, ozonation, appear to be more favourable for the degeneration of azo dye [16–19].

Among different AOPs, the heterogeneous photocatalytic procedures will effectively decrease a wide variety of contaminant in ambience heat and pressure with no hazardous intermediates produce [20]. The methods are started through the excitation and transferring the electron from the valence bands, where it is occupied of electrons to the unfilled conduction bands. Mechanism of photocatalysis shown in Equations 1–3 [21]. The hydroxyl radicals and superoxide radical anions are main oxidising agents in photocatalysis process [22].



In last decades, much interesting has been specified to a sonochemical degeneration of the organic pollutants in liquid environment. The sonochemistry particularly consists of the chemical impacts made by ultrasound once the sound waves is distributed over a liquid solution [23]. For example, in heterogeneous catalytic systems, the usage of an ultrasound makes condition of increased turbulence inside fluid, hence lessening mass transfer limitation and rising the available surface area because of the catalytic fragmentation and de-agglomeration [24]. However, this framework does not attain whole mineralisation thru little irradiation time, because of the creation of hydrophilic intermediate product, reaction volume and instability of the contaminant are the major barriers that put the sonolysis non-productive while usage as alone system [23,25]. So, the arranging of sonolysis per other advance oxidation processes have been utilised to dissolve a limitation of the single sono-chemical degeneration processes [25]. By add ultrasound to the photocatalytic process, mass exchange value is improved and the blocked sites on the

photocatalyst are released [26]. The synchronous use of ultrasound and photocatalysis, named as sonophotocatalysis that has been studied regarding process efficiency to disintegrate different types of organics in model solutions as well as known as one of the powerful AOPs [24]. Moreover, sonophotocatalysis referred to the heterogeneous systems represent the grouping between the visible light and UV, ultrasounds, as well as catalytic process.

Among various semiconductors (ZnO, CdS, SnO<sub>2</sub> etc.), titanium dioxide (TiO<sub>2</sub>) is one of the most efficient and widely used photocatalyst for the degradation of pollutants in aqueous suspension [27]. TiO<sub>2</sub> has been observed to be the maximum effect for the photocatalytic and sonophotocatalytic experiments due to the photostability, obtainability, rather biologically inert, little operation temperatures, little energy consumption, wide photo-catalytic effectiveness, appropriate flat band potential, wide chemical steadiness, water insolubility in maximum ecological state then prevention the creation of unwanted by-products [2]. Moreover, TiO<sub>2</sub> can be degraded organic substance completely into CO<sub>2</sub> and water through irradiation of TiO<sub>2</sub> by ultraviolet light under 400 nm [21]. In spite of wholly advantages of TiO<sub>2</sub>, two main limits in the photo-catalytic activity which are as follows:

- (1) ) Its activation just in the UV amount under 387 nm (3.2 eV)
- (2) ) A significant amount of electron-gap recombination.

To overcome limitations of TiO<sub>2</sub> as a photocatalyst, different of technique can be used to enhance its photocatalytic activity. The doping to TiO<sub>2</sub> with metal ions will establish a new energy level which reduces the band gap and inhibits electron-hole recombination, so improves the absorption of visible light [28,29]. To improve the photocatalytic activity under each light type, TiO<sub>2</sub>-based Ag was suggested being the utmost attractive in the relation to photocatalytic production, cost-effectual, facilities of preparing, etc [20]. On the other hand, the activity of photocatalysts next to recover and recycle must be considered as well as concern to separation after photocatalysis/sonophotocatalysis degeneration, magnetic TiO<sub>2</sub>-based photocatalysts have newly produced interests. Mostly, these magnetic photocatalysts can be recuperated simply by adopting exterior magnetic forces. Some studies for dye removal with Ag-doped TiO<sub>2</sub> and magnetic catalysts (with Fe<sub>3</sub>O<sub>4</sub>) are summarised in Table 1.

In this study, photochemical deposition method was used to prepare silver doped TiO<sub>2</sub> nanoparticle. The photochemical deposition method is very advantageous because

**Table 1.** Dye removal efficiency of Ag/TiO<sub>2</sub> and Ag/TiO<sub>2</sub>/Fe<sub>3</sub>O<sub>4</sub> catalysts synthesised with different methods.

Catalyst	Synthesis method	Dye	Light source	Percentage of removal	Reference
Ag/TiO <sub>2</sub>	Photochemical reduction	Methylene blue	Natural full spectrum lamp	97.1%	[32]
Ag/TiO <sub>2</sub>	With water/oil microemulsion	Methyl orange	Simulated visible light	38.52%	[20]
Ag/TiO <sub>2</sub>	Hydrothermal gel	Methyl orange	UV lamp (365 nm)	79.49%	[30]
Ag/TiO <sub>2</sub> /Fe <sub>3</sub> O <sub>4</sub>	With water/oil microemulsion	4-Chlorophenol	UV-C lamp	82.13%	[31]
			UV-A lamp	83.12%	
Ag/TiO <sub>2</sub> /Fe <sub>3</sub> O <sub>4</sub>	Solvothermal and tyrosine-reduced	Methylene blue	Xe lamp (350–1100 nm)	90%	[34]

Ag/TiO<sub>2</sub> is prepared in one step, fewer chemicals used, shorter duration and cost-effective. Furthermore, the production time was shortened and a more homogeneous catalyst was obtained. Co-precipitation method was used to synthesise Ag/TiO<sub>2</sub>/Fe<sub>3</sub>O<sub>4</sub> magnetic photocatalyst. The removal efficiency of Reactive Red 195 (RR195) dye, used commonly in textile industry, was investigated with photocatalysis and sonophotocatalysis processes using photocatalyst synthesised.

## 2. Materials and methods

### 2.1. Materials

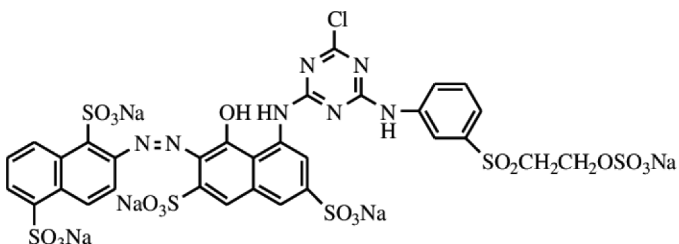
Nano-sized TiO<sub>2</sub> titanium(IV)oxide (Degussa P25, 50 m<sup>2</sup>/g, 75% anatase and 25% rutile), silver nitrate (AgNO<sub>3</sub>), ammonium hydroxide (NH<sub>4</sub>OH, 30% V/V aqueous solution) were purchased from Sigma Aldrich. Hexadecyl-trimethylammonium bromide ([C<sub>16</sub>H<sub>33</sub>)N(CH<sub>3</sub>)<sub>3</sub>]Br, CTAB), n-pentane (C<sub>5</sub>H<sub>12</sub>), ferrous sulphate heptahydrate (FeSO<sub>4</sub>·7H<sub>2</sub>O), ferric chloride (FeCl<sub>3</sub>) and n-hexane (CH<sub>3</sub>(CH<sub>2</sub>)<sub>4</sub>CH<sub>3</sub>) were purchased from Merck KGaA. UV LED lamps (10 W for each lamp, 365 nm wavelength) and visible LED lamps (10 W for each lamp, daylight) were used for light source. Reactive Red 195 was chosen as a model compound due to its extensive use in the textile, paper and ink industries. The chemical structure of RR195 dye is given in Table 2.

### 2.2. Synthesis

Ag-doped TiO<sub>2</sub> synthesis was carried out using photochemical deposition method based on [32] with some modifications. In an exemplary to prepare Ag/TiO<sub>2</sub>, TiO<sub>2</sub> particles were added in 50 mL AgNO<sub>3</sub> solution; then the mixture left to vigorously stirring. NH<sub>4</sub>OH solution was used to set the pH approximately around 10–11. After that, the mixture was irradiated by using a black light blue UV lamp (GE, 15 W) with stirring for 4–5 h in the dark at room temperature. Ag-doped TiO<sub>2</sub> was then dried at 80°C approximately 12 h. Finally, dark purplish Ag/TiO<sub>2</sub> photocatalyst was produced.

Magnetic nanoparticles were produced by employing a co-precipitation technique based on [20] with some modifications. FeSO<sub>4</sub>·7H<sub>2</sub>O (9.34 g, 14 mmol), FeCl<sub>3</sub> (7.8 g, 28 mmol) and NH<sub>4</sub>OH was dispersed to the water/oil microemulsion solution.

**Table 2.** Chemical structure of reactive red 195.

Structure of dye	Molecular weight (g/mol)	$\lambda_{\max}$ nm
 <p style="text-align: center;">Reactive Red 195 M/e = 1136</p>	1136.32	540

Microemulsion represented by CTAB as the surfactant, 1-pentanol as the co-surfactant, as well as hexane as the oil phase. The mixture was sonicated for 30 min and then HNO<sub>3</sub> was used to set the pH of the mixture to about 5. Afterwards, Ag-doped TiO<sub>2</sub> was dispersed and the mixture was stirred for 10 h. Then, the mixture was dried at 100°C. Finally, the magnetic Ag/TiO<sub>2</sub>/Fe<sub>3</sub>O<sub>4</sub> photocatalyst was produced.

### **2.3. Characterisation of the photocatalysts**

X-ray diffraction analysis was carried out with Bruker D8 Advance XRD Analyser in Selcuk University Advanced Technology Research and Application Centre. The diffraction peaks were recorded in the 2θ range between 10° and 90° and used to determine the structures of the samples. The surface morphologies of the prepared catalysts were examined by scanning electron microscope (Zeiss Evo LS10) and transmission electron microscope (TEM). Fourier transform infrared spectroscopy (Bruker Wertex70 FT-IR Spectrometer) analyses were performed to identify catalyst bonds.

### **2.4. Apparatus**

In the apparatus used for photocatalysis and sonophotocatalysis experiments, it is contemplated that the degradation process would be carried out on a movable plate in the range of 0–300 rpm instead of a magnetic stirrer or vertical shaft mechanical stirring, because of magnetic properties of catalyst. This unit allows the placement of six 1-litre beakers in an ultrasonic bath made of stainless steel and the beakers are secured with special holders. Ultrasonic vibrations can be applied with 35 KHz power to beakers. There are covers prepared for each beaker and UV-A (365 nm) and visible (sunlight) PCB LED lamps in the covers can be applied to light beakers with maximum of 30 Watt power. Light power can be adjusted in the 0–30 Watt range by adjusting from the control panel. The cooling structures were added to the covers so that the light sources in the covers did not affect the experimental environments. Moreover, each time can be controlled separately.

### **2.5. Photocatalysis and sonophotocatalysis experiments**

Reactive Red 195 (RR195) dye was chosen as a model compound to evaluate the photocatalytic properties of Ag/TiO<sub>2</sub> and Ag/TiO<sub>2</sub>/Fe<sub>3</sub>O<sub>4</sub>. The aqueous suspensions were stirred in the dark for 25 minutes before the photodegradation tests, thereby achieving the adsorption stability. The photocatalytic reaction was carried out at room temperature (25 ± 2°C) and the distance to the lamp was maintained at about 15 cm. In each photodegradation test, photocatalysts were added to the RR195 solution at an initial concentration of 25 mg/L in a volume of 250 mL under continuous stirring at 150 rpm with a shaker to ensure homogeneity. The initial pH of the solution was adjusted by adding HCl or NaOH solutions, depending on the purpose of the experiments. The concentration of RR195 in the samples was made by 10, 20, 30 min UV-A light irradiation and 2 hours at intervals of 30, 60, 90 and 120 minutes for visible light irradiation after adsorption process in the dark for 25 minutes. For quantitative analysis of RR195 concentration, approximately 3 mL of sample was taken from the mixture of photocatalyst and RR195, followed by centrifugation for Ag/TiO<sub>2</sub> and by usage of an external magnet for

Ag/TiO<sub>2</sub>/Fe<sub>3</sub>O<sub>4</sub>, to separate the photocatalyst particles from the solution. The absorbance of the obtained RR195 solution was then measured at 540 nm with UV-Vis spectrophotometer (Hach DR-2800) to examine the rate of degradation as a function of photocatalytic reaction time under UV-A and visible light irradiation. Finally, photodegradation and sonophotodegradation efficiencies (D%) were calculated according to the Eq.4.

$$D\% = \frac{C - C_t}{C} \times 100 \quad (4)$$

Here C and C<sub>t</sub> are the concentrations of RR195 before and after degradation.

### 3. Result and discussion

#### 3.1. XRD analysis

Phase identification for the doped catalysts are performed using the XRD device that shown in the Figure 1. XRD diffraction patterns of the prepared Ag/TiO<sub>2</sub>; shifting to the right indicates that doping occurs in TiO<sub>2</sub> molecules [33]. Silver deposition on the TiO<sub>2</sub> is also confirmed by the peak at 2θ = 37.35° and 63.07° with the crystal phases of silver [34,35]. The 2θ refraction angles in the range of 10° and 80° show four dominant peaks at 25.66°, 38.14°, 48.38°, and 55.40° associated with different diffraction planes attributed to the anatase phase of P25 TiO<sub>2</sub> [33,36]. While, peaks at 27.79°, 36.44°, 41.5°, and 54.27° with different diffraction planes attributed to the rutile phase of TiO<sub>2</sub> [33,35]. Further, additional peaks at 2θ = 31.05° and 53.01° appeared after iron was added to the prepared Ag/TiO<sub>2</sub>, it showed the presence of Fe<sub>3</sub>O<sub>4</sub> magnetic nanoparticle and successfully doped onto Ag/TiO<sub>2</sub> [37–39]. Peaks corresponding to FeTiO<sub>3</sub> were also observed at 2θ = 23.17°, 32.86°, and 40.19° [35,40]. Furthermore, a Fe/Ti mixed oxide has a hexagonal structure containing two thirds of the octaheric position occupied by the cations [40]. FeTiO<sub>3</sub> can be produced in a liquid mixture using the citrate gel technique during catalyst synthesis and by different methods such as H<sub>2</sub>/H<sub>2</sub>O reduction or co-precipitation. The two Fe<sup>3+</sup> ions in α-Fe<sub>2</sub>O<sub>3</sub> are replaced by Fe<sup>2+</sup> and Ti<sup>4+</sup> along the vertical crystallographic axis. Reported that FeTiO<sub>3</sub>/TiO<sub>2</sub> has a wider bandwidth and has a better yield than pure TiO<sub>2</sub> [20].

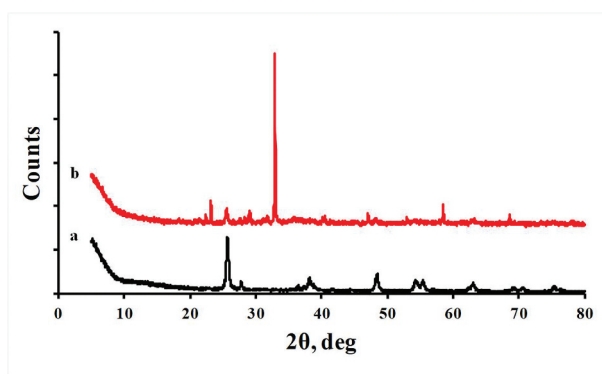
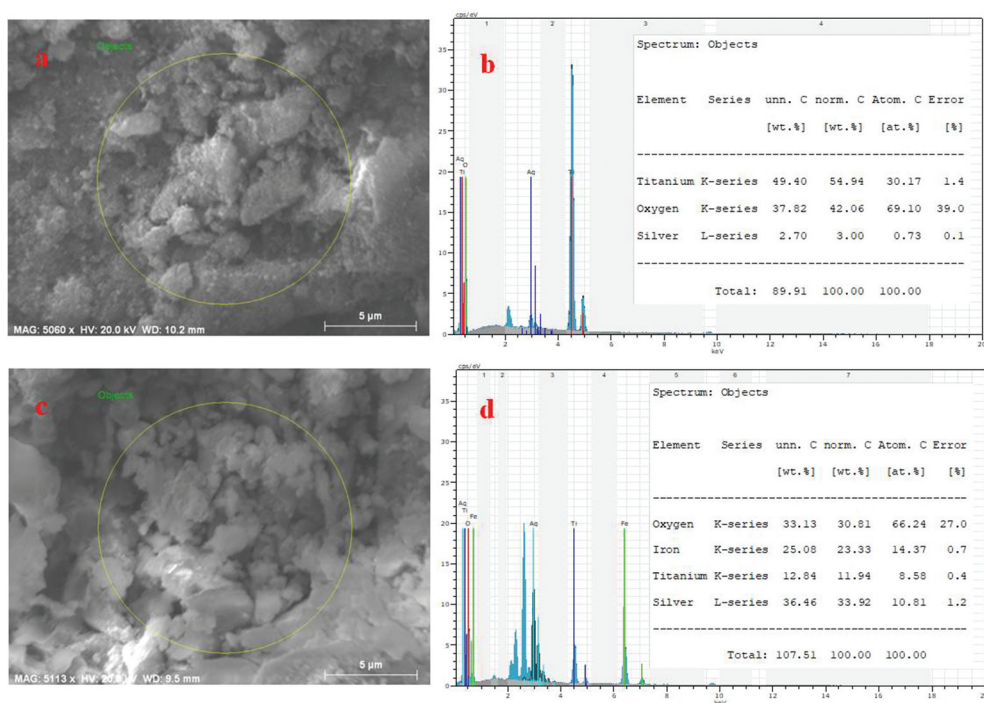


Figure 1. A) Ag/TiO<sub>2</sub> b) Ag/TiO<sub>2</sub>/Fe<sub>3</sub>O<sub>4</sub> photocatalysts XRD spectrum.





**Figure 2.** A,b) Ag/TiO<sub>2</sub>, c,d) Ag/TiO<sub>2</sub>/Fe<sub>3</sub>O<sub>4</sub> photocatalysts SEM-EDX analysis.

### 3.2. SEM, TEM and EDX Analysis

SEM, TEM and EDX analysis of Ag/TiO<sub>2</sub> and Ag/TiO<sub>2</sub>/Fe<sub>3</sub>O<sub>4</sub> are shown in Figures 2 and 3. In SEM analysis, Ag/TiO<sub>2</sub> catalyst prepared by the photochemical deposition method consists of small amorphous particles, which exhibits lower agglomeration and has more uniform shape and size particles. In the EDX analysis of the prepared Ag/TiO<sub>2</sub>, the ratio of Ag, Ti and O<sub>2</sub> was 3.00%, 54.94% and 42.06%, indicating the presence of Ag nanoparticle in the sample.

In SEM analysis, Ag/TiO<sub>2</sub>/Fe<sub>3</sub>O<sub>4</sub> prepared by co-precipitation method, has a sharp-edged crystal structure and cracks and protrusions on its surface. In EDX analysis, it shows an additional peak representing 23.33% iron. Thus, Ag supported magnetic TiO<sub>2</sub> was successfully prepared.

### 3.3. FT-IR analysis

FT-IR spectroscopy for TiO<sub>2</sub> coated with magnetic nanoparticles in the range of (500–3500 cm<sup>-1</sup>) is related to the formation of the Fe-O functional group and is well matched to the characteristic peak at 601 cm<sup>-1</sup> Figure 4 [39,41]. 821 cm<sup>-1</sup> and 890 cm<sup>-1</sup> are related to the two peaks surrounding Ti-O-Ti bond, and the absorption peak at 988 cm<sup>-1</sup> corresponds to the vibration of Ti-O-C[41–43]. The two peaks at 1035 cm<sup>-1</sup> and 1076 cm<sup>-1</sup> result from the C-O tension vibration [44]. Peaks around 1313 cm<sup>-1</sup> and 1396 cm<sup>-1</sup> for the TiO<sub>2</sub>-coated magnetic sample can only be attributed to the presence of



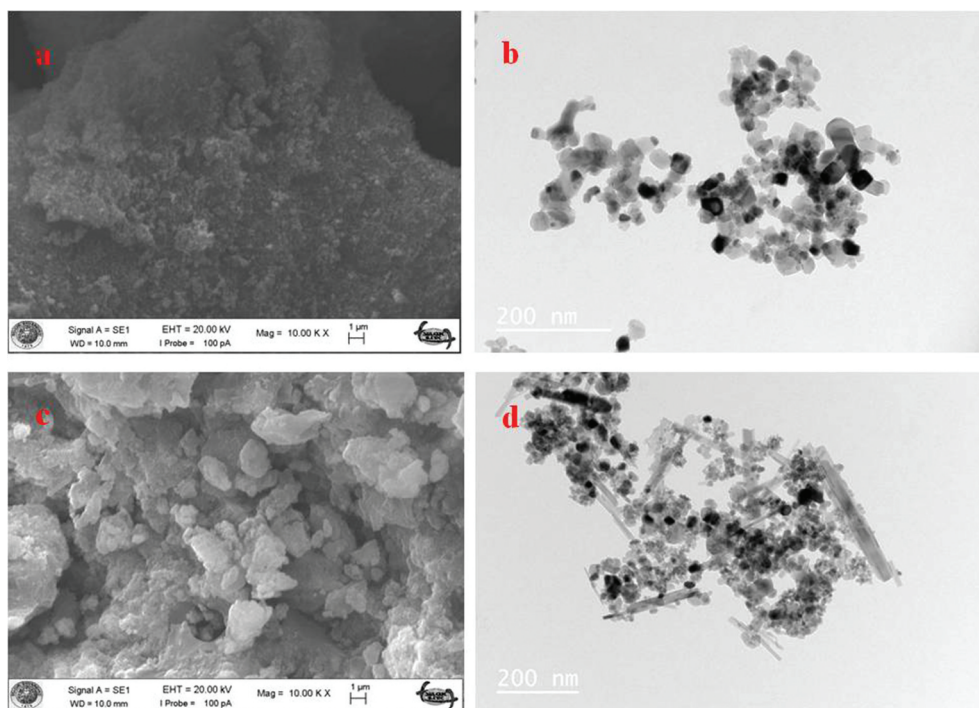


**Figure 3.** **A,b)** Ag/TiO<sub>2</sub>, **c,d)** Ag/TiO<sub>2</sub>/Fe<sub>3</sub>O<sub>4</sub> photocatalysts SEM-TEM analysis.

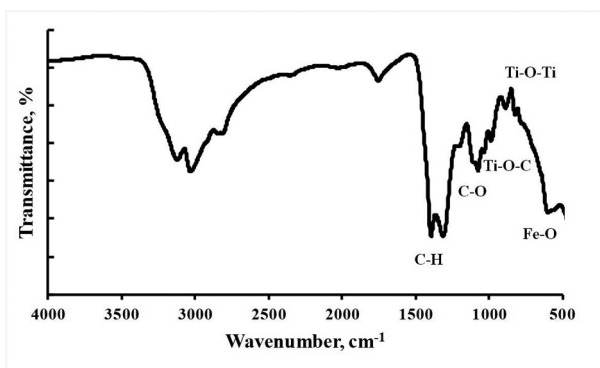


**Figure 4.** Ag/TiO<sub>2</sub>/Fe<sub>3</sub>O<sub>4</sub> FT-IR spectroscopy analysis.

C-H tensile vibrations [39,44]. Silver used in the doped TiO<sub>2</sub> catalyst did not result in any significant changes in the FT-IR spectrum [33].

### **3.4. Photocatalysis processes**

#### **3.4.1. The effect of irradiation time**

While the removal of RR195 dye with TiO<sub>2</sub> was 22% for 30 min irradiation time under UV-A light, it increased to 33% with Ag-doped TiO<sub>2</sub> by photochemical deposition method. Due

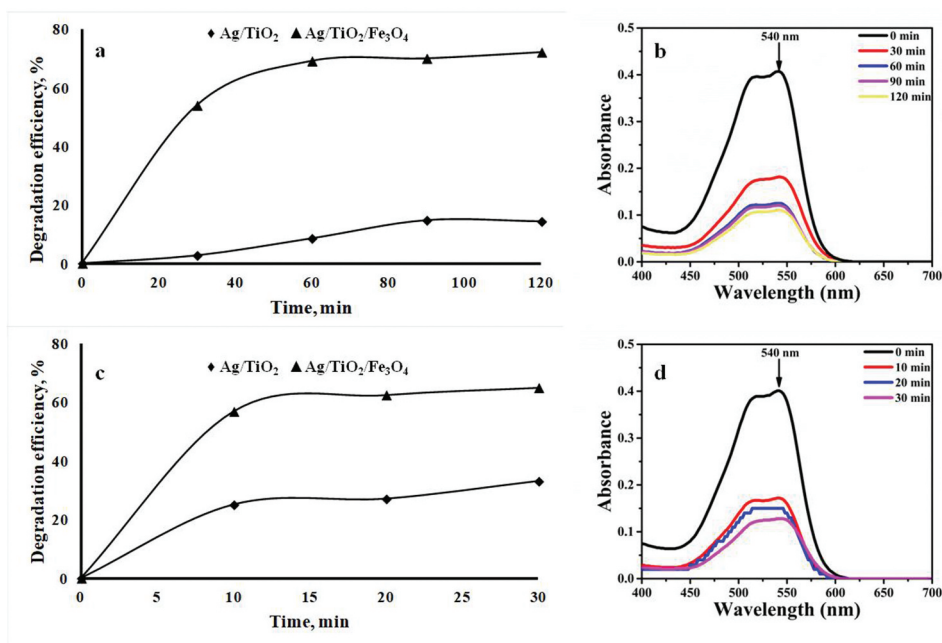


**Figure 5.** The effect of time on the photodegradation and absorbance of RR195 in the presence of Ag/TiO<sub>2</sub>/Fe<sub>3</sub>O<sub>4</sub> under **a,b**) visible light, **c,d**) UV-A light irradiation.

to this increase observed in batch experiments, photodegradation of RR195 was investigated in the presence of only Ag/TiO<sub>2</sub> and Ag/TiO<sub>2</sub>/Fe<sub>3</sub>O<sub>4</sub> catalysts for different irradiation time. The effect of irradiation time on the photodegradation and absorbance change of RR195 is shown in Figure 5. The results, after the saturated solution of RR195 containing the photocatalyst is mixed in the dark (without illumination), show that it exhibited that the adsorption of RR195 to the catalyst surface did appear to be insignificant. Under both visible and UV-A light, photocatalytic degradation of RR195 increased with increasing irradiation time. When Ag/TiO<sub>2</sub> was used as the photocatalyst, the degradation at the 120 minute irradiation of visible light was found to be 14.3% but was 33% during 30 minute irradiation of UV-A. Photodegradation in the presence of magnetic Ag/TiO<sub>2</sub>/Fe<sub>3</sub>O<sub>4</sub> was found to be 72% at 120 min of visible light, however, the degradation was 65%, for 30-min in UV-A irradiation. This is due to the interaction of the dye molecule with the surface of the photocatalyst. Increased duration of illumination has also increased the interaction so the photodegradation efficiency of photocatalyst is increased [45]. The synthesised magnetic Ag/TiO<sub>2</sub>/Fe<sub>3</sub>O<sub>4</sub> composite photocatalyst, in this study, different photocatalytic activity and synergistic interactions between different catalysts Ag, TiO<sub>2</sub> and Fe<sub>3</sub>O<sub>4</sub> tested under visible light irradiation and UV-A light showed the same experimental conditions. Because of these interactions, the transfer and separation of photo-generated electrons and voids are facilitated and this significantly increases photocatalytic performance. RR195 dye contains naphthalene rings, azo bond and vinyl sulphone groups; these bonds are cleaved by the active sites of catalyst and leading to generation of smaller aromatic organic structures [46]. As the TiO<sub>2</sub> content of the

photocatalyst enhances, the number of active sites and subsequently, the generation of hydroxyl radicals ( $\text{OH}\cdot$ ) would be increased. By trapping electrons, Ag can effectively facilitate electron-hole separation and enhance electron production on  $\text{TiO}_2$  surface, thus increasing the photocatalytic activity [47].

### 3.4.2. The effect of initial pH and dye concentration

The effect of the solution initial pH on the performance of the magnetic  $\text{Ag}/\text{TiO}_2/\text{Fe}_3\text{O}_4$  composite synthesised for the degradation of RR195 was evaluated. Photocatalytic experiments were carried out at initial pH values ranging from 3 to 9 for RR195 initial concentration 25 mg/L, temperature  $25^\circ\text{C}$ , catalyst amount 0.1 g/L, and light intensity 27 W. The irradiation time was taken as 30 min and 120 min, for UV-A and visible light, respectively. The pH of the RR195 solution was adjusted using 0.1 M hydrochloric acid and 0.1 M sodium hydroxide solutions to reach the desired pH values and after pH adjustment the catalyst was added. The results of these experiments are presented in Figure 6. Our results exhibited that removal efficiency of RR195 was higher at low initial pH values under the same experimental conditions [20,48]. After 120 min of illumination with visible light, the RR195 degradation efficiency of the magnetic  $\text{Ag}/\text{TiO}_2/\text{Fe}_3\text{O}_4$  photocatalyst was obtained as 72.5% when the initial pH of the solution was 3, and 72.1% and 52% when the pH was increased to 6 and 9, respectively. The degradation obtained by the synthesised magnetic  $\text{Ag}/\text{TiO}_2/\text{Fe}_3\text{O}_4$  photocatalyst under UV-A irradiation for 30 min was 70%, 65% and 52% for the initial solution pH 3, 6 and 9, respectively. A further effect of solution pH on dye photo-degradation is the surface ionisation state of the catalyst, as well as the formation of hydroxyl radicals by reaction between positive cavities and hydroxide ions [48]. As a result, the degradation efficiency of RR195 is significantly affected by the initial solution pH; as the initial solution pH decreased and the maximum degradation reached pH 3. Theoretically, RR195 reactive dye is anionic, so the conversion efficiency is higher at low pH because of the electrostatic attraction between anionic dye and positively-charged  $\text{TiO}_2$  [49].

To observe the effect of the initial concentration of RR195 (ranging from 0.025 to 0.045 g/L) on degradation, photocatalysis experiments were carried out using  $\text{Ag}/\text{TiO}_2/\text{Fe}_3\text{O}_4$  photocatalyst at fixed initial conditions ( $25^\circ\text{C}$  temperature, 0.1 g/L catalyst dose, 27 W light intensity, pH 6 value) under UV-A and visible light for 30 min and 120 min, respectively. The change in photocatalytic degradation due to the initial concentration of the dye in the presence of photocatalyst for both visible and UV-A light is given in

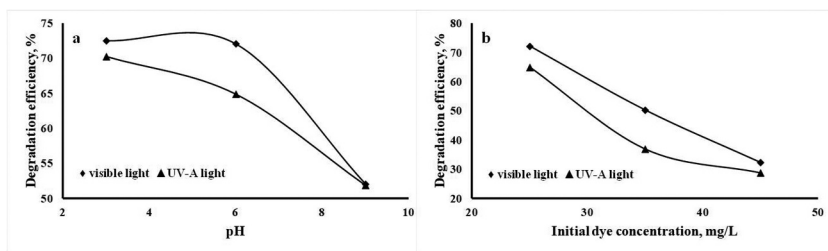


**Figure 6.** The effect of initial pH and dye concentration the photodegradation of RR195 in the presence of  $\text{Ag}/\text{TiO}_2/\text{Fe}_3\text{O}_4$  under **a)** visible, **b)** UV-A light irradiation.

**Figure 6.** For  $\text{Ag}/\text{TiO}_2/\text{Fe}_3\text{O}_4$  with initial dye concentrations of 0.025, 0.035 and 0.045 g/L, the degradation of RR195 yield was 72, 50 and 32% after illumination for 120 min under visible light, respectively. After 30-min UV-A illumination, it was determined to be 65, 37 and 29% for initial dye concentrations of 0.025, 0.035 and 0.045 g/L. The increase in dye concentration leads to a decrease in photocatalytic rate constant [20,45,48]. According to previous studies, the rate of photocatalytic degradation relates to the number of hydroxyl radicals formed on the catalyst surface and the likelihood of these radicals reacting with dye molecules. Therefore, at higher dye concentrations, the formation of OH radicals on the surface of the catalyst decreases as the active sites are occupied by the dye molecules [45,48,50]. Thus, the degradation rate increased with initial concentration increased.

### 3.4.3. The effect of light source

After 30 minutes of illumination with UV-A light, the RR195 degradation efficiencies of the synthesised magnetic  $\text{Ag}/\text{TiO}_2/\text{Fe}_3\text{O}_4$  photocatalyst were obtained as 61, 57 and 65%, respectively, while the powers were 9, 18 and 27 W. According to the results obtained, it can be said that the strength of the UV light irradiation source affects the degradation of the dye in the aqueous solution using  $\text{Ag}/\text{TiO}_2/\text{Fe}_3\text{O}_4$ . Moreover, after 120 min of illumination with visible light, the RR195 degradation efficiencies of the synthesised magnetic  $\text{Ag}/\text{TiO}_2/\text{Fe}_3\text{O}_4$  photocatalyst were obtained as 68, 72 and 73%, respectively, while the powers were 9, 18 and 27 W. The results show that light power plays an important role in the degradation of RR195. Basically, the degradation efficiency increases with the UV radiation intensity, thereby increasing the excitation of the photocatalyst particles to form higher electron gap pairs. The holes decompose the pollutants absorbed on the surface of the photocatalyst and oxidise the water to form free radicals. Moreover, the increase in the hydroxyl radical degrades the contaminated materials in the solution [2].

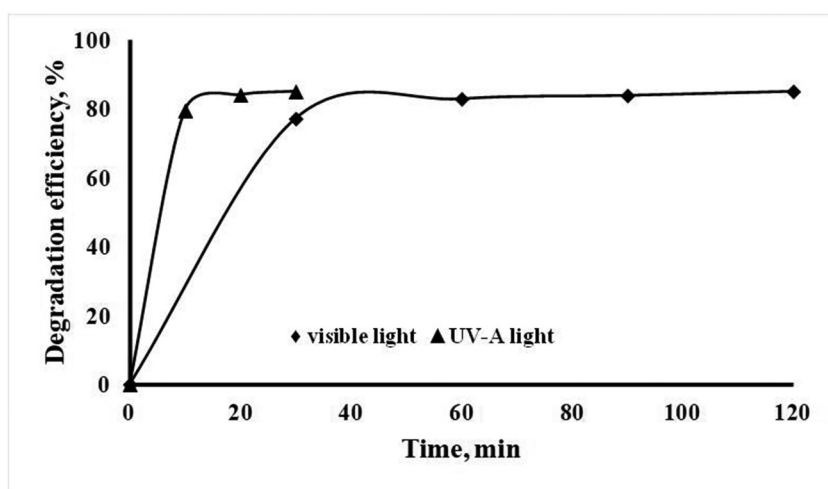


**Figure 7.** The effect of time on the sonophotodegradation of RR195 in the presence of  $\text{Ag}/\text{TiO}_2/\text{Fe}_3\text{O}_4$  under visible and UV-A light irradiation.

### 3.5. Sonophotocatalysis process

#### 3.5.1. The effect of irradiation time

In the presence of  $\text{Ag}/\text{TiO}_2/\text{Fe}_3\text{O}_4$ , sonophotodegradation of RR195 dye was investigated under different irradiation effects. The effect of irradiation time on sonophotocatalysis of RR195 is shown in Figure 7. Under both visible and UV-A light, sonophotocatalytic degradation of RR195 increased with increasing irradiation time. All parameters selected for this study (initial concentration of dye, temperature, amount of catalysis, pH, amplitude of ultrasound energy and light intensity) were kept constant. When sonophotocatalysis test was performed with  $\text{Ag}/\text{TiO}_2/\text{Fe}_3\text{O}_4$  approximately 79% degradation was achieved in the first 10 minutes of UV-A irradiation light, however, photocatalytic testing with UV-A alone yielded 57%. After 30 minutes of UV irradiation, the values obtained as 65% and 85% for photocatalysis and sonophotocatalysis, respectively. In addition, sonophotodegradation of RR195 was 85% in irradiation with 120 min of visible light, however, the degradation at the 120 min irradiation of visible light alone was 72% using magnetic  $\text{Ag}/\text{TiO}_2/\text{Fe}_3\text{O}_4$ . This is due to the interaction of the dye molecule with the surface of the photocatalyst. Increased duration of illumination has also increased the interaction. As a result, sonophotocatalysis efficiency of photocatalyst increases [23,45,51].

#### 3.5.2. Comparison of photocatalysis and sonophotocatalysis processes

When the photocatalysis and sonophotocatalysis processes are combined, a significant effect on the removal of pollutants can be seen [23,24,51]. In the present study, the removal of RR195 dye was obtained as approximately 85% after 30 min of UV-A light irradiation at sonophotocatalysis process with the uses of  $\text{Ag}/\text{TiO}_2/\text{Fe}_3\text{O}_4$ . While the same process was carried out only by photocatalysis, the removal of RR195 dye was 72% Figure 8. After 120 minutes of visible light irradiation, the values were obtained as 65% for photocatalysis and 85% for sonophotocatalysis, respectively. This makes

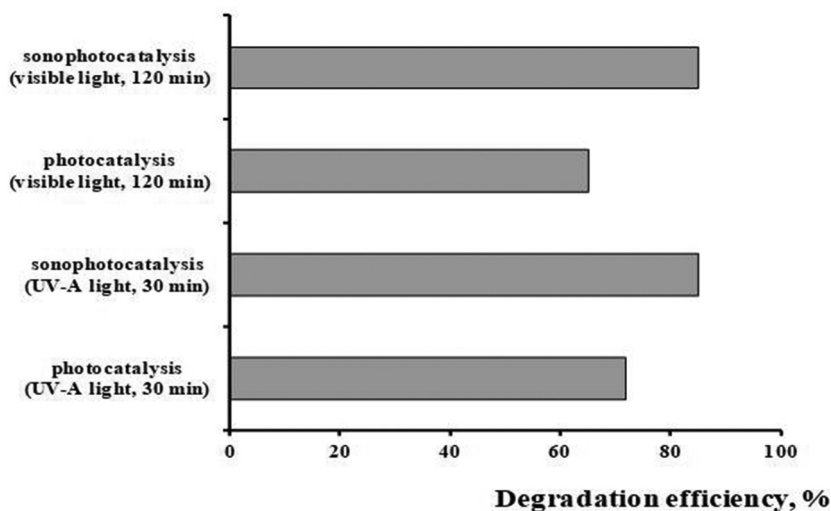


**Figure 8.** The comparison of photocatalysis and sonophotocatalysis of RR195 in the presence of  $\text{Ag}/\text{TiO}_2/\text{Fe}_3\text{O}_4$  under visible and UV-A light irradiation.

sonophotocatalysis faster than photocatalysis. The main mechanism for the removal of RR195 by sonophotocatalysis has resulted in increased  $\bullet\text{OH}$  production in the RR195 solution due to the combined sonolysis and photocatalysis processes [23,24,51]. Another major reason is to increase the catalyst surface mass transfer in the dye solution [23,24,51]. It is also important to mention that catalyst activity is increased due to ultrasound separation of nanoparticles, which increase the surface area of the catalyst [23,24,51]. When all the results are combined, it is proposed that degradation of reactive dyes such as RR195 can be achieved effectively by a combination of advanced oxidation processes in the presence of  $\text{Ag}/\text{TiO}_2/\text{Fe}_3\text{O}_4$ , UV-A, visible light and sonolysis.

#### 4. Conclusion

In this study, Ag and  $\text{Fe}_3\text{O}_4$  were bound with  $\text{TiO}_2$  to increase the activity of the catalyst and to facilitate separation from the solution. The photochemical deposition method used is very advantageous to other chemical methods, because  $\text{Ag}/\text{TiO}_2$  is prepared in one step, fewer chemicals used, shorter duration and cost-effective. Furthermore, the production time was shortened and a more homogeneous catalyst was obtained. Analyzes of XRD, SEM, EDX, and FT-IR were performed to examine the structure of the catalysts prepared for this study. In XRD graph of the  $\text{Ag}/\text{TiO}_2/\text{Fe}_3\text{O}_4$  catalyst displayed four anatase  $\text{TiO}_2$  peaks, five rutile peaks, two Ag peaks, and two  $\text{Fe}_3\text{O}_4$  peaks. However, the influences of different factors on photocatalysis and sonophotocatalysis methods were investigated. For example, photocatalytic degradation of RR195 under the time effect increased with increasing irradiation time. So, photodegradation of  $\text{Ag}/\text{TiO}_2/\text{Fe}_3\text{O}_4$  was 72% at 120-min irradiation of visible light but was 65% for 30 min after UV-A irradiation. Moreover, after sonophotocatalyst was added the degradation of  $\text{Ag}/\text{TiO}_2/\text{Fe}_3\text{O}_4$  was 85% after irradiated with UV-A for 30 min and reached the same value when irradiated with visible light for 120 min. Sonophotocatalysis processes have been more described, due to its a significant effect on the removal of contaminants. In the literature, the main mechanism for the removal of RR195 by sonophotocatalysis has an increased free radical  $\bullet\text{OH}$  production in the solution. Magnetic properties facilitated the separation of the catalyst from RR195 solution after photocatalysis/sonophotocatalysis, in addition to enabling separation by an external magnet instead of separate equipment such as centrifugation.

#### Disclosure statement

No potential conflict of interest was reported by the author(s).

#### References

- [1] E. Jafarnejad and J. Nemati, *Anal. Chem. Lett* **5**, 192 (2015). doi:10.1080/22297928.2015.1129289.
- [2] H. Zangeneh, A. Zinatizadeh, M. Habibi, M. Akia and M.H. Isa, *J. Ind. Eng. Chem* **26**, 1 (2015). doi:10.1016/j.jiec.2014.10.043.
- [3] A. Abul, S. Samad, D. Huq, M. Moniruzzaman and M. Masum, *J. Textile Sci. Eng* **5**, 2 (2015).



- [4] T. Yonar, in *Advances in Treating Textile Effluent*, edited by P.J. Hauser (InTech, Rijeka, Croatia, 2011).
- [5] M.S. Cebeci and T. Torun, *Treatment of Textile Wastewater Using Nanofiltration*, presented at the 6th Eurasian Multidisciplinary Forum, Vienna, Austria, 2017.
- [6] A.S. Sartape, A.M. Mandhare, V.V. Jadhav, P.D. Raut, M.A. Anuse and S.S. Kolekar, *Arab. J. Chem* **10**, 3229 (2017). doi:10.1016/j.arabjc.2013.12.019.
- [7] F. Kehinde and H.A. Aziz, *Int. J. Innovative Res. Sci. Eng. Technol* **3**, 15310 (2014). doi:10.15680/IJRSET.2014.0308034.
- [8] K. Bharathi and S. Ramesh, *Appl. Water Sci* **3**, 773 (2013). doi:10.1007/s13201-013-0117-y.
- [9] N. Daneshvar, A. Khataee, M. Rasoulifard and M. Pourhassan, *J. Hazard. Mater.* **143**, 214 (2007). doi:10.1016/j.jhazmat.2006.09.016.
- [10] S.S. Moghaddam, M.A. Moghaddam and M. Arami, *J. Hazard. Mater.* **175**, 651 (2010). doi:10.1016/j.jhazmat.2009.10.058.
- [11] S. Nataraj, K. Hosamani and T. Aminabhavi, *Desalination* **249**, 12 (2009). doi:10.1016/j.desal.2009.06.008.
- [12] M. Oden and S. Kucukconggar, *Global Nest J* **20**, 234 (2018).
- [13] M.F. Sevimli and H.Z. Sarikaya, *J. Chem. Technol. Biotechnol.* **77**, 842 (2002). doi:10.1002/jctb.644.
- [14] A. Yasar and S. Yousaf, *Global Nest J* **14**, 477 (2012).
- [15] F. Temel, M. Turkylmaz and S. Kucukconggar, *Eur. Polym. J.* **125**, 109540 (2020). doi:10.1016/j.eurpolymj.2020.109540.
- [16] S.-H. Kim, H.H. Ngo, H. Shon and S. Vigneswaran, *Sep. Purif. Technol.* **58**, 335 (2008). doi:10.1016/j.seppur.2007.05.035.
- [17] B. Neppolian, H.C. Choi, S. Sakthivel, B. Arabindoo and V. Murugesan, *J. Hazard. Mater.* **89**, 303 (2002). doi:10.1016/S0304-3894(01)00329-6.
- [18] B. Gözmen, M. Turabik and A. Hesenov, *J. Hazard. Mater.* **164**, 1487 (2009). doi:10.1016/j.jhazmat.2008.09.075.
- [19] S. Sultana, M.Z. Khan, K. Umar, A.S. Ahmed and M. Shahadat, *J Mol Struct* **1098**, 393 (2015). doi:10.1016/j.molstruc.2015.06.032.
- [20] W.J. Chung, D.D. Nguyen, X.T. Bui, S.W. An, J.R. Banu, S.M. Lee, S.S. Kim, D.H. Moon, B.H. Jeon and S.W. Chang, *J. Environ. Manage.* **213**, 541 (2018). doi:10.1016/j.jenvman.2018.02.064.
- [21] M.R.D. Khaki, M.S. Shafeeyan, A.A.A. Raman and W.M.A.W. Daud, *J. Environ. Manage* **198**, 78 (2017).
- [22] A. Dar, K. Umar, N. Mir, M. Haque, M. Muneer and C. Boxall, *Res. Chem. Intermed* **37**, 567 (2011). doi:10.1007/s11164-011-0299-6.
- [23] M.A.N. Khan, M. Siddique, F. Wahid and R. Khan, *J. Ultrason. Sonochem* **26**, 370 (2015). doi:10.1016/j.ultsonch.2015.04.012.
- [24] S. Kavitha and P. Palanisamy, *Int. J. Civ. Environ. Eng* **3**, 1 (2011).
- [25] A. Shokri, *Arch. Hyg. Sci* **5**, 229 (2016).
- [26] M. May-Lozano, V. Mendoza-Escamilla, E. Rojas-García, R. López-Medina, G. Rivadeneyra-Romero and S.A. Martinez-Delgado, *J. Clean. Prod.* **148**, 836 (2017). doi:10.1016/j.jclepro.2017.02.061.
- [27] M. Oves, M.Z. Khan and I.M. Ismail, editors, *Modern Age Environmental Problems and Their Remediation* (Springer International Publishing, Cham, Switzerland, 2018).
- [28] K. Umar, M.N.M. Ibrahim, A. Ahmad and M. Rafatullah, *Res. Chem. Intermed* **45**, 2927 (2019). doi:10.1007/s11164-019-03771-x.
- [29] K. Umar, T. Parveen, M.A. Khan, M.N.M. Ibrahim, A. Ahmad and M. Rafatullah, *Desalin. Water Treat* **161**, 275 (2019). doi:10.5004/dwt.2019.24298.
- [30] Y. Zhang, F. Fu, Y. Li, D. Zhang and Y. Chen, *Nanomaterials* **8**, 1032 (2018). doi:10.3390/nano8121032.
- [31] S. Chang, W. Chung, S. Yu and S. Lee, *Desalin. Water Treat* **54**, 3646 (2015). doi:10.1080/19443994.2014.923207.
- [32] S. Ko, C.K. Banerjee and J. Sankar, *J. Compos. Part B: Eng* **42**, 579 (2011). doi:10.1016/j.compositesb.2010.09.007.



- [33] S. Sowmya, G. Madhu and M. Hashir, *IOP Conf. Ser.: Mater. Sci. Eng.* **310**, 012026 (2018). doi:10.1088/1757-899X/310/1/012026.
- [34] L. Zhang, Z. Wu, L. Chen, L. Zhang, X. Li, H. Xu, H. Wang and G. Zhu, *J. Solid State Sci* **52**, 42 (2016). doi:10.1016/j.solidstatesciences.2015.12.006.
- [35] J. Tang, R. Wang, M. Liu, Z. Zhang, Y. Song, S. Xue, Z. Zhao and D.D. Dionysiou, *Chem. Eng. J* **351**, 1056 (2018). doi:10.1016/j.cej.2018.06.171.
- [36] J. Zhan, H. Zhang and G. Zhu, *Ceram. Inter* **40**, 8547 (2014). doi:10.1016/j.ceramint.2014.01.069.
- [37] K.-H. Choi, S.-Y. Park, B.J. Park and J.-S. Jung, *J. Surf. Coat. Technol* **320**, 240 (2017). doi:10.1016/j.surfcoat.2017.01.029.
- [38] X. Jia, R. Dai, D. Lian, S. Han, X. Wu and H. Song, *J. Appl. Surf. Sci* **392**, 268 (2017). doi:10.1016/j.apsusc.2016.09.014.
- [39] M. Abbas, B.P. Rao, V. Reddy and C. Kim, *J. Ceram. Int* **40**, 11177 (2014). doi:10.1016/j.ceramint.2014.03.148.
- [40] P. García-Muñoz, G. Pliego, J. Zazo, A. Bahamonde and J. Casas, *J. Environ. Chem. Eng* **4**, 542 (2016). doi:10.1016/j.jece.2015.11.037.
- [41] K. Tedsree, N. Temnuch, N. Sriplai and S. Pinitsoontorn, *J. Mater. Today: Proc* **4**, 6576 (2017).
- [42] M. Ye, Q. Zhang, Y. Hu, J. Ge, Z. Lu, L. He, Z. Chen and Y. Yin, *J. Chem.–A Eur. J* **16**, 6243 (2010). doi:10.1002/chem.200903516.
- [43] J. Wei, C. Leng, X. Zhang, W. Li, Z. Liu and J. Shi, *J. Phys. Conf. Ser* **149**, 012083 (2009).
- [44] Z.-D. Li, H.-L. Wang, X.-N. Wei, X.-Y. Liu, Y.-F. Yang and W.-F. Jiang, *J. J. Alloys Compd* **659**, 240 (2016). doi:10.1016/j.jallcom.2015.10.297.
- [45] K. Azad and P. Gajanan, *J. Chem. Sci. J* **8**, 164 (2017).
- [46] Z. Han, J. Li, X. Han, X. Ji and X. Zhao, *Chem. Eng. J* **358**, 176 (2019). doi:10.1016/j.cej.2018.09.224.
- [47] N. Aghajari, Z. Ghasemi, H. Younesi and N. Bahramifar, *J. Environ. Health Sci. Eng* **17**, 219 (2019). doi:10.1007/s40201-019-00342-5.
- [48] B. Chládková, E. Evgenidou, L. Kvítek, A. Panáček, R. Zbořil, P. Kovář and D. Lambropoulou, *J. Environ. Sci. Pollut. Res* **22**, 16514 (2015). doi:10.1007/s11356-015-4806-y.
- [49] X.N. Pham, D.T. Pham, H.S. Ngo, M.B. Nguyen and H.V. Doan, *Chem. Eng. Commun* **2020**, 1. doi:10.1080/00986445.2020.1712375
- [50] M. Rauf and S.S. Ashraf, *J. Chem. Eng. J* **151**, 10 (2009). doi:10.1016/j.cej.2009.02.026.
- [51] T. Yetim and T. Tekin, *J. Period. Polytech. Chem. Eng* **61**, 102 (2017).